J Low Temp Phys (2011) 163: 284–301
DOI 10.1007/s10909-011-0350-4

Expansion or Contraction of Slit Pores Due to Gas Uptake

F. Ancilotto · M.W. Cole · A. Grosman · E.S. Hernández · F. Toigo

Received: 27 December 2010 / Accepted: 30 January 2011 / Published online: 17 February 2011

Abstract Adsorption inside a slit pore of flexible width w is explored, with a focus on how w varies as a function of the external pressure P of a gas in equilibrium with the adsorbate within the pore. The analysis is first carried out in general, using a minimization of the thermodynamic grand potential energy of the system. This leads to an equation predicting both the gas uptake N as a function of chemical potential μ and the expansion (or contraction) of the pore in response to the adsorbate's pressure. The resulting equilibrium behavior depends on the elastic parameters of the host material. Explicit results are derived for three adsorption systems: a low density fluid, Ar (a classical fluid at finite temperature T) in a graphite pore and ^{4}He within a Au pore at $T = 0$. The resulting behaviors include some situations where the pore expands and others for which it contracts. The difference arises from the sign of the thermodynamic response of the fluid as a function of slit width.

F. Ancilotto · F. Toigo (✉)
Department of Physics, University of Padua, via Marzolo 8, Padua, Italy
e-mail: toigo@pd.infn.it

F. Ancilotto
e-mail: franc@pd.infn.it

M.W. Cole
Department of Physics, Penn State University, University Park, PA 16802, USA
e-mail: miltoncole@aol.com

A. Grosman
Institut des NanoSciences de Paris, Université Pierre et Marie Curie, UMR7588, 4 Place Jussieu, 75005 Paris, France
e-mail: annie.grosman@insp.jussieu.fr

E.S. Hernández
Departamento de Física, Facultad de Ciencias Exactas y Naturales, Universidad de Buenos Aires, and Consejo Nacional de Investigaciones Científicas y Técnicas, 1428 Buenos Aires, Argentina
e-mail: shernand@df.uba.ar

Keywords Physisorption in pores · Capillary condensation · Imbibition

1 Introduction

A familiar phenomenon is the contraction of a sponge when it has dried out or its expansion when it becomes fully saturated with water. Similar phenomena are known to occur for materials with microscopic or mesoscopic porosity when fluids are imbibed [1–22]. One consequence of this behavior is that a fundamental quantity, the adsorption surface area, becomes ambiguous; the area concept must be generalized to include the effects of material expansion or contraction. Except in those circumstances where these effects are known to be negligible, from the perspective of the statistical mechanics and thermodynamics of adsorption, the relaxation of the adsorbent should be taken into account [23–26]. From an experimental point of view, it has been shown how the elastic strains induced by gas adsorption are significantly modified by an external constraint applied to a porous material [27, 28].

Except in the case of crystalline adsorbents, like metal-organic-framework materials or zeolites, the challenge of predicting adsorption is particularly difficult due to irregularity of the substrate. Quite generally, the computational problem involving relaxation is compounded by the need for the analysis to include simultaneously both the adsorbate and the adsorbent in the calculations.

Motivated by recent calculations by Günther et al. [25, 26], this paper addresses a relatively simple geometry, the slit pore, for the case of an unspecified, but parameterized, host material. Our goal is to determine the equilibrium behavior (the density and thermodynamic variables) of the fluid for a generic slit pore. This problem is simplified by the fact that there exists just one geometrical degree of freedom characterizing the porous environment: the pore width w. First, we describe the problem as a free energy minimization with respect to w. Specifically, we write the grand potential energy $\Omega(\mu, w)$ as a sum of three terms:

$$\Omega(\mu, w) = F_{sub}(w) + F_{fluid}(N; w) - \mu N \tag{1}$$

Throughout a given set of calculations presented here, the temperature T is held fixed, so we omit that variable from the equations. Of course, all relevant functions and variables (other than the chemical potential μ which is an independent variable) will depend on T in any explicit numerical calculation. The first term in (1), $F_{sub}(w)$, is the Helmholtz free energy of the host material, which we do not specify, except that in some cases we will employ an expansion about the equilibrium value (w_0) prior to gas uptake:

$$F_{sub}(w) = F_0 + \left(\frac{\lambda A}{2}\right)(w - w_0)^2 \tag{2}$$

The constant F_0 and the elastic coefficient λ are parameters characterizing the slit. A is the (one-side) surface area of the slit, for which we will take the thermodynamic limit. We note in passing that these three parameters include, in principle, all thermodynamic fluctuations, including those involving slits of spatially varying width $w(x, y)$. Equation (1) is an adiabatic approximation, which implicitly omits coupling

between the pore's fluctuations and those of the film. In (1), $F_{fluid}(N; w)$ is the Helmholtz free energy of the adsorbed fluid. The number of particles N is an implicit parameter in (1), derived from minimization at fixed w and μ:

$$0 = \left(\frac{\partial \Omega}{\partial N}\right)_{\mu,w} \tag{3}$$

$$0 = \left[\frac{\partial}{\partial N}(F_{fluid}(N; w) - \mu N)\right]_{\mu} \tag{4}$$

Equation (4) is familiar because it is the traditional equation used to compute uptake within an inflexible environment. For any value of $\mu > \mu_{min}$ an uptake threshold value, (4) yields one, or more, solutions of the form $N(\mu; w)$, the total uptake as a function of μ and w. For any specified value of w, one of these solutions will correspond to $\Omega_{film}(\mu, w)$ the lowest grand free energy of the film, the function in braces in (4). We express the corresponding uptake as $N_{equilib}(\mu; w)$. The remaining problem is then to minimize (with respect to w) the function

$$\Omega_{equilib}(\mu, w) = F_{sub}(w) + \Omega_{film}(\mu, w) \tag{5}$$

Hence, we arrive at the final equation describing the general condition for equilibrium

$$(\partial/\partial w)\, F_{sub}(w) = -(\partial/\partial w)\, \Omega_{film}(\mu, w) \tag{6}$$

Equation (6) is the equilibrium mechanical condition for a confined fluid: the normal force exerted by the fluid on the wall equals the force exerted by the wall on the fluid. For that reason, the right hand side of (6), when divided by the area A of the wall, is a thermodynamic pressure, which we call P_{wall}; this function of μ and w is defined by:

$$P_{wall} \equiv -(\partial/\partial w)\,(\Omega_{film}(\mu, w)/A) = (\partial/\partial w)\,(F_{sub}(w)/A) \tag{7}$$

While (7) is a necessary (local) condition for equilibrium, there exists an additional global condition, the minimization of the functional in (1).

For any system to which the harmonic approximation, (2), applies, (7) yields a change in pore width Δw:

$$\Delta w \equiv w - w_0 = P_{wall}/\lambda \tag{8}$$

Note that P_{wall} is sometimes set equal to the sum of the coexisting vapor pressure and the so-called disjoining pressure [29, 30].

The case where $P_{wall} < 0$ is generally described as a *tension*, rather than a pressure; in such a situation, the pore contracts due to adsorption. The thermodynamic driving force in this case is that the free energy $\Omega_{film}(\mu, w)$ is *reduced* by a contraction of the pore. Note, as expected, that a very compliant pore (small λ) exhibits a large change $|\Delta w|$ due to the imbibed fluid. Equation (8) is a general result of linear response theory. It is accurate for small changes of the width from the empty pore value w_0. There are two situations for which (8) is suspect. One is the relatively

mundane case when (2) fails because it omits higher order terms, e.g. Δw^3. The more interesting situation occurs when the uptake contribution $\Omega_{film}(\mu, w)$ drastically shifts the global minimum, far from w_0. Such is the case when the oscillatory dependence of Ω_{film}, due to layering effects, causes a macroscopic change in the uptake. One example studied in our recent work is the imbibition transition when the film coverage jumps discontinuously from zero to a full monolayer [11].

The outline of this paper is the following. In the next section, we evaluate the consequences of the preceding equations in general form and derive a kind of Henry's law of pore expansion in the limit of low coverage of the fluid inside the pore. In Sect. 3, we present results for the case of Ar inside a slit pore of variable width at a range of temperatures that are relevant to typical Ar experiments. In Sect. 4, we address a very different case, liquid ^{4}He at $T = 0$. Section 5 addresses the elastic properties of the adsorbent.

2 Pore Expansion/Contraction in the Henry's Law Regime

2.1 Classical Fluid at Low P

We assume for simplicity that the total potential energy of an adsorbed particle equals a sum of contributions from the two neighboring half-spaces, denoted by subscripts indicating substrate regions $z < 0$ and $z > w$, respectively:

$$V(z) = V_<(z) + V_>(z) \tag{9}$$

For identical substrates we will write $V_<(z) = V_{wall}(z)$ and $V_>(z) = V_{wall}(|z - w|)$. The pressure P_{wall} on a wall is defined in terms the force per unit area, $\mathbf{F_w}/A$, exerted by the fluid on the wall according to $\mathbf{F_w}/A = P_{wall}\hat{\mathbf{n}}$, where $\hat{\mathbf{n}}$ is the unit vector pointing outward from the slit. Taking into account that from Newton's third law it follows that $\mathbf{F_w}$ is the opposite of the force $\mathbf{F_f}$ exerted by the wall on the particles, and that for the wall located at $z = 0$ one has $\hat{\mathbf{n}} = -\hat{\mathbf{z}}$, we get:

$$P_< = -\int dz\, \rho(z)(\partial V_</\partial z) \tag{10}$$

where the integral is over the volume occupied by the film ($0 < z < w$), with density $\rho(z)$. This relation and the preceding equations can be evaluated explicitly in various limits. First, we consider a classical film at very low N and high $T \equiv (1/k_B\beta)$. Then, the density at position z may be written in terms of the gas density outside the pore ($n_{out} = P\beta$) with the barometric formula:

$$\rho(z)/n_{out} = e^{-\beta V(z)} \tag{11}$$

$$P_< = -n_{out}\int dz\, e^{-\beta V(z)}(\partial V_</\partial z) \tag{12}$$

Because of the oppositely directed surface normal, $P_>$, the fluid's pressure on the wall at $z = w$, is the negative of a similar expression, with $V_>$ substituted for $V_<$. By

symmetry, in the case of identical substrate on the two sides of the pore $P_< = P_> = P_{wall}$, which is proportional to P. The ratio P_{wall}/P involves an integral, which depends on two different potential energy functions:

$$P_{wall}/P = -\beta \int dz\, e^{-\beta V(z)} (\partial V_</\partial z) \tag{13}$$

We note in passing the result of (13) in the academic case of an infinitely wide pore. Then, the derivative is nonzero only in a region (the range of the adsorption potential) near $z = 0$, for which $V(z) \to V_<(z)$. Then (for the case of an essentially hard wall potential), the integration yields unity. Hence, the pressure at the wall equals that of the coexisting vapor, as expected. The film coverage (not the thermodynamic excess coverage) is given by

$$N/A = \int dz\, \rho(z) = n_{out} \int dz\, e^{-\beta V(z)} = \beta P \int dz\, e^{-\beta V(z)} \tag{14}$$

Thus, the usual Henry's law states that coverage is proportional to P, with a T-dependent proportionality coefficient:

$$N/(PA) = \beta \int dz\, e^{-\beta V(z)} \tag{15}$$

Since both N and P_{wall} are proportional to P, they satisfy $N \propto P_{wall} \propto P$. (The excess coverage is also proportional to P, but the coefficient of proportionality depends upon an arbitrary definition of the pore volume.)

2.2 Quantum fluid at low N

We consider next a very different limit, a quantum fluid at either very low T or $T \equiv 0$. First, let us assume that $T = 0$. There exist two possible ground states, in principle: a gas (e.g. 2D ^{3}He) or a condensed state. In the former case, at very low density $\theta = N/A$, the gas consists of a set of independent particles, by assumption. Then, (9) indicates that P_{wall}/N is a constant at low N which is determined by the single-particle ground-state wave function in the pore, $\psi(z)$, with $\rho(z) = |\psi(z)|^2$. Next, let us assume that the ground state is self-bound, e.g. a liquid ^{4}He monolayer on each surface. At low N, a small number of particles will be condensed within an island of area $< A$, the full area. There will be similar islands on each side of the pore. Each of these particles will exert the same force so that the total force is proportional to N. This statement is true even in the case of capillary condensation, since $\rho(z)$ does not depend on N at $T = 0$. We next consider a low T situation, again focused on the monolayer case. At very low coverage, the film will be a 2D gas, so that the force is proportional to N. At some point the 2D density θ will reach that of condensation, θ_g. In the 2-phase region ($\theta_g < \theta < \theta_c$), where θ_c is the denser phase density, we may write the total number of particles in terms of the areas A_g and A_c covered by the respective phases:

$$N = A_c\theta_c + (A - Ac)\theta_g = A_c(\theta_c - \theta_g) + A\theta_g \equiv A\theta \tag{16}$$

$$A_c/A = (\theta - \theta_g)/(\theta_c - \theta_g) \tag{17}$$

This ratio $A_c/A = 1$, of course, if $\theta_c = \theta$ while $A_c/A = 0$, if $\theta_g = \theta$. The total force per unit area f in the 2-phase region $\theta_g < \theta < \theta_c$ may then be written as a corresponding linear combination, involving $\phi_{g,c}$ the force per unit area of each phase:

$$f A = A_c\phi_c + (A - A_c)\phi_g = A_c(\phi_c - \phi_g) + A\phi_g \tag{18}$$

$$f = (\phi_c - \phi_g)\frac{(\theta - \theta_g)}{(\theta_c - \theta_g)} + \phi_g \tag{19}$$

This force is manifestly a linear function of the total number of particles $N = A\theta$; however, f is *not* simply proportional to N.

3 Ar Fluid in Strongly Attractive Slits at Finite Temperature

We address in this section the adsorption of Argon fluid at finite temperatures within slits of variable widths, whose adsorption potentials mimic a strong adsorbent, e.g. a graphite plane, and compute the pressure exerted by the fluid on the slit walls.

Our starting point is the phenomenological free energy DF of Ref. [31], which has been used to study the wetting properties of Ar on planar surfaces of alkali metals [31] and solid CO_2 [32]. The fluid free energy F is expressed as a functional of the fluid density $\rho(\mathbf{r})$ as:

$$F[\rho] = F_{HS}[\rho] + \frac{1}{2}\int\int \rho(\mathbf{r})\rho(\mathbf{r}')u_{att}(|\mathbf{r} - \mathbf{r}'|)d\mathbf{r}d\mathbf{r}' + \int V_{ext}(\mathbf{r})\rho(\mathbf{r})d\mathbf{r} \tag{20}$$

The first contribution F_{HS} is the free-energy functional for an inhomogeneous hard-sphere reference fluid, the second contribution is the fluid-fluid energy, where u_{att} is the interatomic potential, and the third contribution is the energy due to the interaction with the substrate, where V_{ext} is the external potential for a single Ar atom. The free energy functional F_{HS} is written in terms of a suitable coarse-grained density obtained by averaging the true fluid density over an appropriate local volume, and generates an appropriate triplet-direct-correlation function for the one-component fluid. The inter-particle potential is described by an effective interaction

$$u_{att}(r) = \begin{cases} 0, & \text{if } r \le \lambda^{1/6}\sigma_1 \\ 4\epsilon[\lambda(\sigma_1/r)^{12} - (\sigma_1/r)^6], & \text{if } r > \lambda^{1/6}\sigma_1 \end{cases} \tag{21}$$

which, in the case of Ar fluid, takes the form of the bare Lennard-Jones potential with parameters $\sigma_1 = \sigma_{Ar} = 3.405$ Å and $\epsilon = 119.8$ K when the parameter λ is set to unity. If $\lambda < 1$ the long-range properties remains those of the bare potential, which allows to treat both λ and σ_1 as adjustable parameters of the whole functional. These (temperature-dependent) parameters are fixed in such a way to reproduce the experimental values of coexisting bulk liquid and vapor densities [31].

The equilibrium fluid density in the presence of the slit potential is found from the variation, with respect to the density, of the above free energy functional at a

fixed temperature T. The resulting Euler equation $\mu = \delta F/\delta\rho(\mathbf{r})$ is solved iteratively by using a fictitious first-order damped dynamics, where the value of the chemical potential μ is fixed from the start. At convergence, the actual number of Ar atoms in the slit is found from the equilibrium density profile, $\int \rho(\mathbf{r})d\mathbf{r} = N$.

In the case of Ar in a slit with planar parallel surfaces located at $z = \pm w/2$, the external potential is taken to be $V_{ext}(\mathbf{r}) = V_s(z; w)$ with:

$$V_s(z; w) = V_{wall}(w/2 - z) + V_{wall}(w/2 + z) = V_s(-z; w) \tag{22}$$

and we assume that each wall provides a $9 - 3$ potential of the form $V_{wall}(x) = C_9/x^9 - C_3/x^3$, where $C_9 = 3035.85 \times 10^4$ K Å^9 and $C_3 = 58956$ K Å^3 are chosen so that the well depth and equilibrium distance are 1000 K and 3.4 Å, respectively. In this way the resulting adsorption properties are those of a strong adsorbent like graphite.

We focus on a representative temperature, $T = 128$ K for most of our calculations. The effect of varying T has also been investigated, in which case we considered three different temperatures: $T = 85$ K (i.e. close to the Ar triple point $T_t = 83.8$ K), $T = 120$ K and $T = 140$ K (closer to the Ar critical temperature $T_c = 150.9$ K).

We first address the case of relatively large slits. For a given slit, from the equilibrium density profile we get the pressure P_{wall} exerted by the fluid on the slit wall by using (10). The conversion from the units $K/\text{Å}^3$ shown in the figure to more popular units is $1K/\text{Å}^3 = 138$ bar.

In Fig. 1 we show the pressure as a function of the chemical potential μ. One observes that for low Ar intake (i.e. for very negative μ values) the pressure is positive for all w, resulting in a slit pore expansion. However, at a particular value of μ, corresponding to the capillary condensation (CC) transition [25, 26], a sharp drop in pressure occurs, whose amplitude is larger for smaller slits, and that, at least for not too large slits, is enough to change the sign of P_{wall}, i.e. the pore contracts at

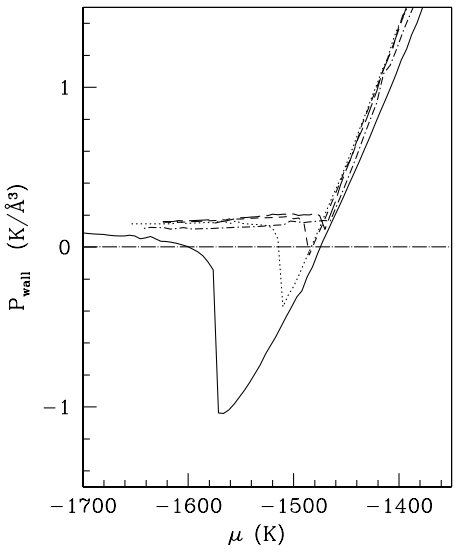

Fig. 1 Pressure on large slit walls. *Solid line*: $w = 30$ Å; *dotted line*: $w = 40$ Å; *short dash line*: $w = 50$ Å; *long dash line*: $w = 70$ Å; *dot-short dash*: $w = 80$ Å

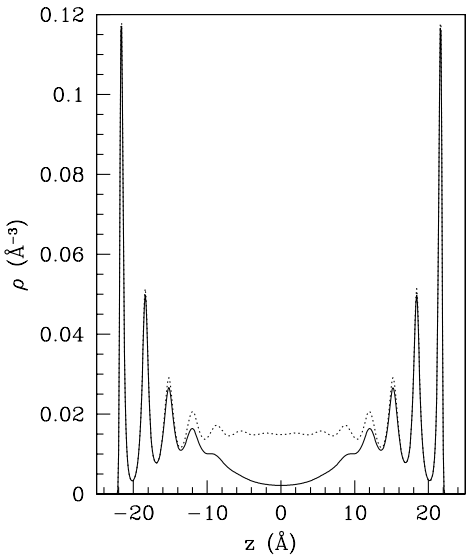

Fig. 2 Equilibrium density profiles in a $w = 50$ Å slit at $T = 128$ K, just before and after the drop in P_{wall}

CC. After the slit becomes filled, the pressure on its walls rises again rapidly towards positive (and large) values, corresponding again to slit expansions.

The magnitude of the discontinuity in pressure at the CC transition may be written as $\Delta P_{wall} \simeq \Delta N \langle -dV/dz \rangle$ where ΔN is the number of particles per unit area involved in the CC and $\langle -dV/dz \rangle$ is the average z-component of the force on the particles in the region filled by CC. This force is negative and of large magnitude for the case of small pores, decreasing with w increasing.

Note that the difference $|\mu_0 - \mu|$ decreases by increasing w and, for larger slits, although a kink is still visible in P_{wall} at CC, the drop in pressure becomes smaller, but P_{wall} is never negative.

In Fig. 2 we show the computed density profiles within the $w = 50$ Å slit, immediately before and after the sharp drop in P_{wall} visible in Fig. 1, clearly showing that this drop occurs exactly at CC. A similar behavior was found in the Monte Carlo calculations of Günther et al. [25, 26].

A quite different behavior is observed, however, for narrower slits. Our results are shown in Fig. 3. Note the differences in the vertical scale with respect to Fig. 1. Now the negative pressure exerted on the slit walls is much larger, but the pressure drop is no longer as sharp as occurs for wider slits. This difference is related to the fact that for such small slits there is no real CC transition due to the limited space available between the slit walls, not enough to accommodate a true liquid phase. Another important difference with respect to the case of large slits is that at low Ar intake the pressure is always negative, i.e. narrow slits under such conditions tend to shrink even at very low Ar coverages.

Figure 4 shows the computed grand potential density as a function of the Ar chemical potential. The slope of Ω satisfies $(\partial\Omega/\partial\mu)_T = -N$. Hence there is a slope discontinuity, when CC occurs. This is evident for larger slits, whereas the discontinuity disappears for smaller slits, again showing that no real CC transition occurs in this

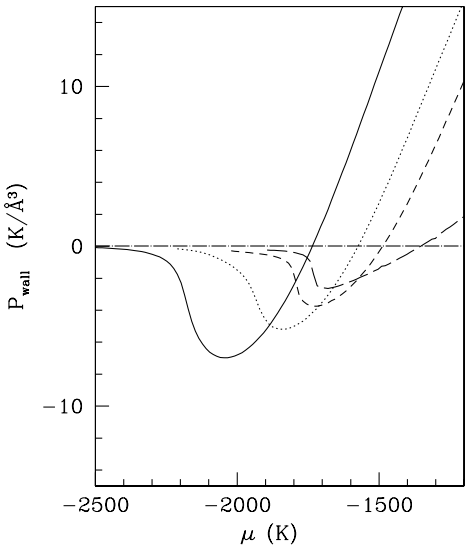

Fig. 3 Pressure on narrow slit walls. *Solid line*: $w = 12$ Å; *dotted line*: $w = 15$ Å; *short dash line*: $w = 18$ Å; *long dash line*: $w = 20$ Å

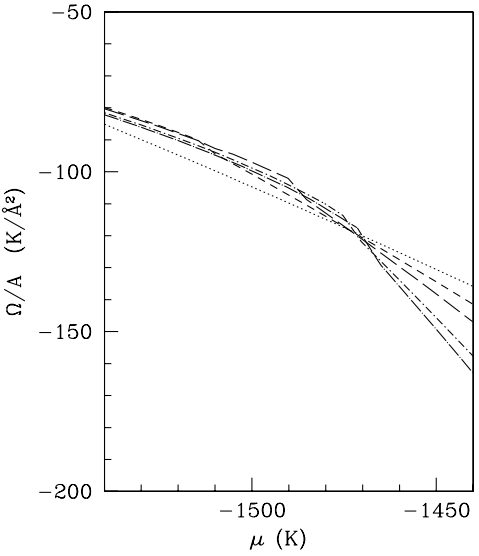

Fig. 4 Grand potential density for different slit widths. *Solid line*: $w = 30$ Å; *dotted line*: $w = 40$ Å; *short dash line*: $w = 50$ Å; *long dash line*: $w = 70$ Å; *dot-short dash*: $w = 80$ Å

case. The disappearance of CC has been noticed earlier in Monte Carlo simulations of classical and quantum fluids in small pores and slits [33–35].

Finally, we studied how the pressure exerted on the slit walls changes with temperature. This is shown in Fig. 5, for the case $w = 30$ Å, at three representative temperatures, $T = 85$, 120 and 140 K. It appears that the sharp drop in P_{wall} at CC is decreased in value and smoothed out at higher T, and that the location of the CC transition shifts towards saturation pressure as the temperature is increased, as predicted by Kelvin's equation for capillary condensation in a slit geometry [36]. Ex-

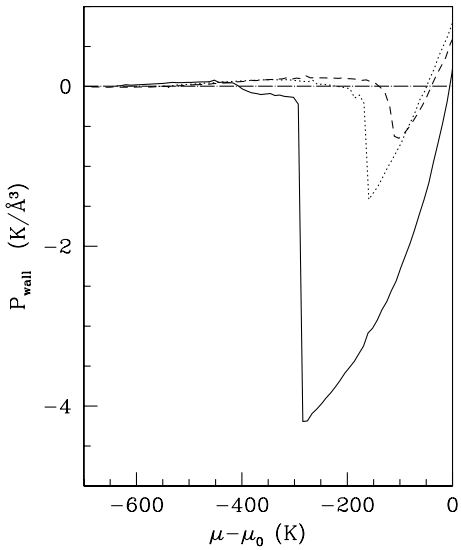

Fig. 5 Pressure on the slit walls ($w = 30$ Å) at different temperatures. *Solid line*: $T = 85$ K; *dotted line*: $T = 120$ K; *short dash line*: $T = 140$ K. μ_0 is the chemical potential at liquid vapor coexistence at each temperature

perimentally, upward shifts with temperature of the capillary transition value of μ are known [37]. Finally, we mention that adsorption/desorption isotherms near capillary filling of a slit pore show metastable branches in the "gas" and liquid portions, resulting in hysteretic loops. We do not address here the effect of hysteresis on expansion/contraction of the slit pore but rather point out that the location of the jump in P_{wall} towards negative values will shift, in the desorption branch, towards less negative values of the chemical potential.

4 Helium in Narrow Gold Slits at Zero Temperature

We now address a very different system, ^{4}He confined within a pore bounded by Au at $T = 0$. The behavior in this case will bear some similarity to that found in the previous section for Ar, an entirely classical fluid. The reason is that the phenomena in question are sensitive to size effects associated with the pore width.

While these calculations could, in principle, be carried out for any confining surfaces, we have chosen Au as typical in its attraction to He. With an adsorption depth $D = 112.5$ K (for a single surface), this substrate is intermediate between the very attractive graphite surface and much less attractive adsorbents, such as Mg and alkali metals [38]. At $T = 0$, the density functional used to determine energies and density profiles is the well-known Orsay-Trento functional [39] that contains the kinetic energy of the quantum fluid, a core-suppressed Lennard-Jones (LJ) interaction between He atoms, and a density-dependent correlation term. The density profile $\rho(z; w)$ is obtained for each separation w by solving a nonlinear, integrodifferential Schrödinger-like equation

$$\left[-\frac{\hbar^2}{2m}\nabla^2 + V[\rho] + V_s(z; w)\right]\sqrt{\rho} = \mu\sqrt{\rho} \tag{23}$$

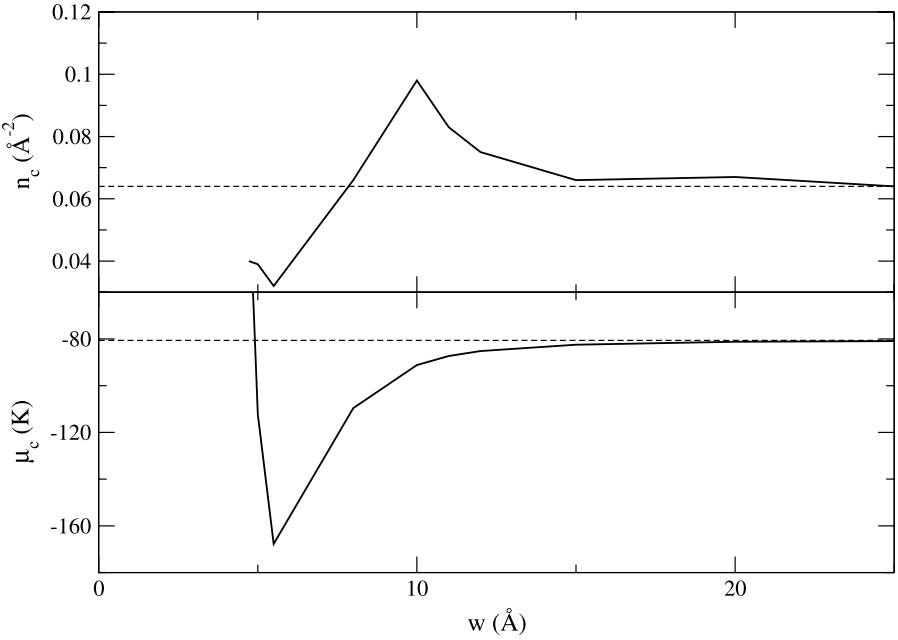

Fig. 6 *Upper panel*: coverage n_c at submonolayer condensation as a function of wall separation w. *Lower panel*: same for the chemical potential μ_c

with $V[\rho]$ the total mean field and V_s the substrate potential. Here the chemical potential μ is the energy eigenvalue for fixed coverage $n = N/A$. The calculations in this work for the one dimensional fluid are performed as reported, i.e. in Refs. [40, 41]. The substrate potential $V_s(z; w)$ is of the same form as in (22) but with $C_9 = 4896.4 \times 10^2$ K Å^9 and $C_3 = 3471$ K Å^3 so that V_{wall} exhibits a minimum located at $x_{min} = 2.74$ Å with the above indicated depth $D = 112.5$ K.

On semi-infinite Au, helium condenses with a submonolayer condensation transition to a liquid of density $n_c = 0.032$ Å^{-2} and chemical potential $\mu_c = -80.6$ K, above which it undergoes a layering sequence with peaks spaced by about 2.7 Å. Above six layers the fluid reaches essentially the bulk density $\rho_0 = 0.022$ Å^{-3}. In the case of two facing walls, ^{4}He is unbound (relative to bulk) at separations lower than 4.7 Å; for slightly wider pores, a bound single layer appears at the center of the slit, which splits into two peaks at around $w = 7$ Å. For increasing separation the condensed fluid follows a layering sequence with the same periodicity of a single wall. The corresponding values of (μ_c, n_c) are plotted as functions of w in Fig. 6. While the chemical potential smoothly approaches the infinite separation limit, the coverage at condensation undergoes oscillations that reflect the capacity of the pore to accommodate new central layers.

Figures 7 and 8 respectively display the total energy (per unit surface) and grand potential Ω_{film} (per unit surface) of the condensed helium fluid as a function of chemical potential μ for several widths. The interesting aspect in this figure is the multiple curve crossing, as predicted in Ref. [25, 26]. In fact, the force per unit area

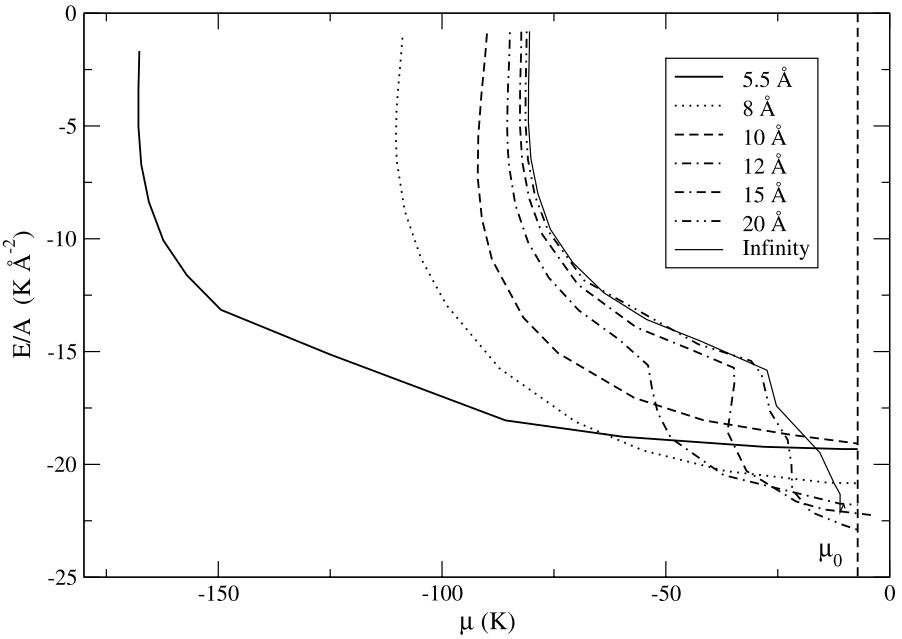

Fig. 7 Total energy (per unit surface of either wall) as a function of chemical potential for several narrow to moderate widths

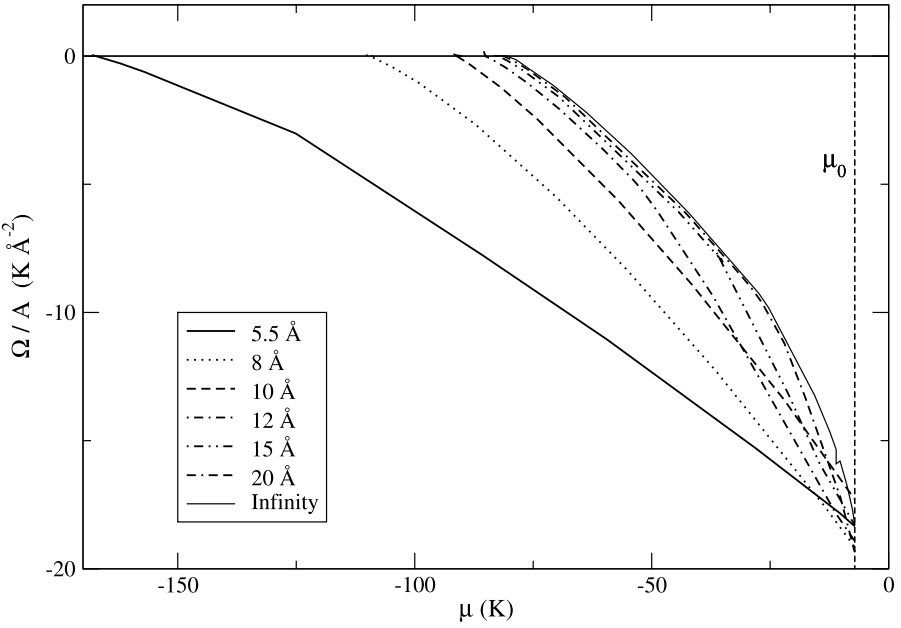

Fig. 8 Same as Fig. 7 for the total grand potential

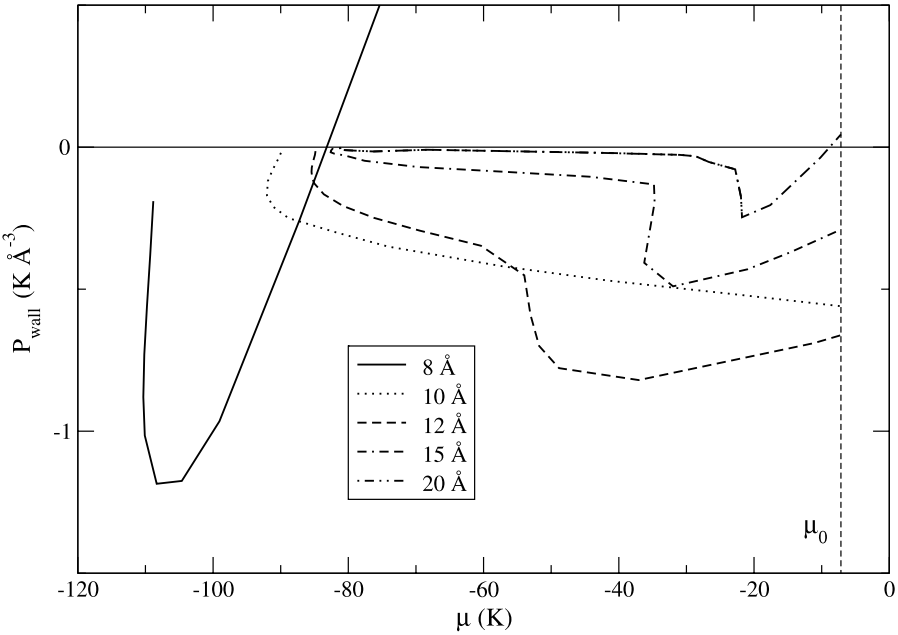

Fig. 9 Same as Fig. 7 for the pressure on either wall

for each width can be computed as

$$P_{wall} = -\int_{-w/2}^{w/2} dz\, \frac{\partial V_s}{\partial w}\, \rho(z; w)$$
$$\equiv -\int_{-w/2}^{w/2} dz\, V'_{wall}(|z - w/2|)\, \rho(z; w) \qquad (24)$$

due to the reflection symmetry of the density profiles, thus coincident with (10). This quantity is plotted in Fig. 9 for the same slits displayed in Figs. 7 and 8.

The variation of P_{wall} can be understood analyzing the contents of the convolution integral in (24). For this purpose, we show several density profiles in Figs. 10, 11, 12, 13, labeled by coverage on top of the potential (full line) and the local force $f(z; w) = -\partial V_s(z, w)/\partial w$ exerted by a particle at z on both walls (dashed).

Let us first analyze Fig. 10. We note that for the lowest coverages, the density "fills" the slit, thus exploiting most of the attractive part of the force; in fact, this density distribution is the remnant of the unique central layer that occurs in narrower pores. When the coverage increases and the two layers become well defined, they move towards the walls and pick up most of the repulsion. For the 12 Å case in Fig. 11, the peaks remain well defined near the walls and the balance is a negative convolution. The kink in the curve in Fig. 9 corresponds to the appearance of the third central layer and lies in the region of an almost vanishing local force. We note that a similar kink appears for $w = 15$ Å; moreover, for this width one appreciates in Fig. 7, the appearance of a van der Waals-like loop near $\mu = -35$ K, that reveals

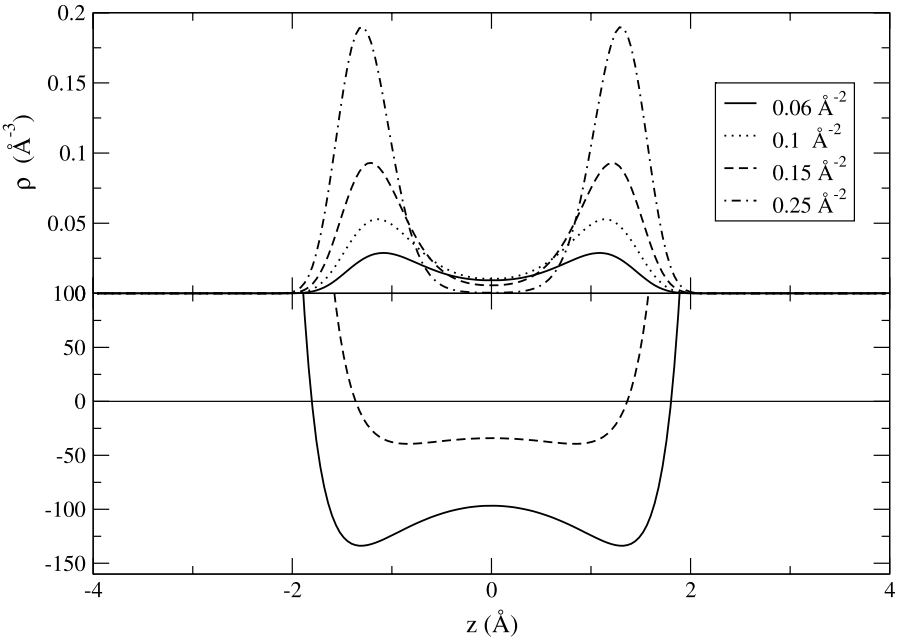

Fig. 10 *Upper panel*: density profiles in a slit of width 8 Å as a function of position. *Lower panel*: substrate potential (*full line*) and local force (*dashed line*) exerted by a single helium atom on both walls

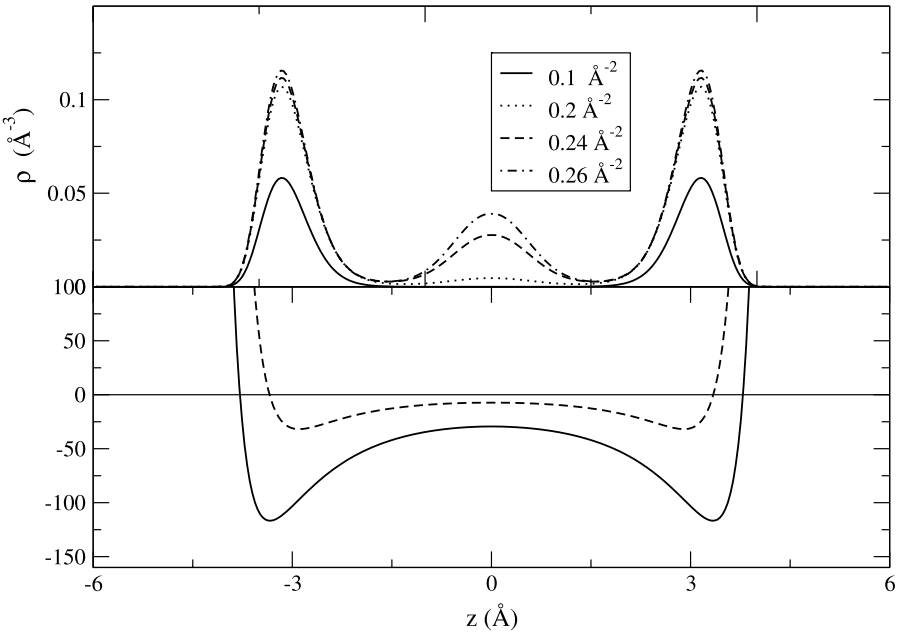

Fig. 11 Same as Fig. 10 for a width of 12 Å

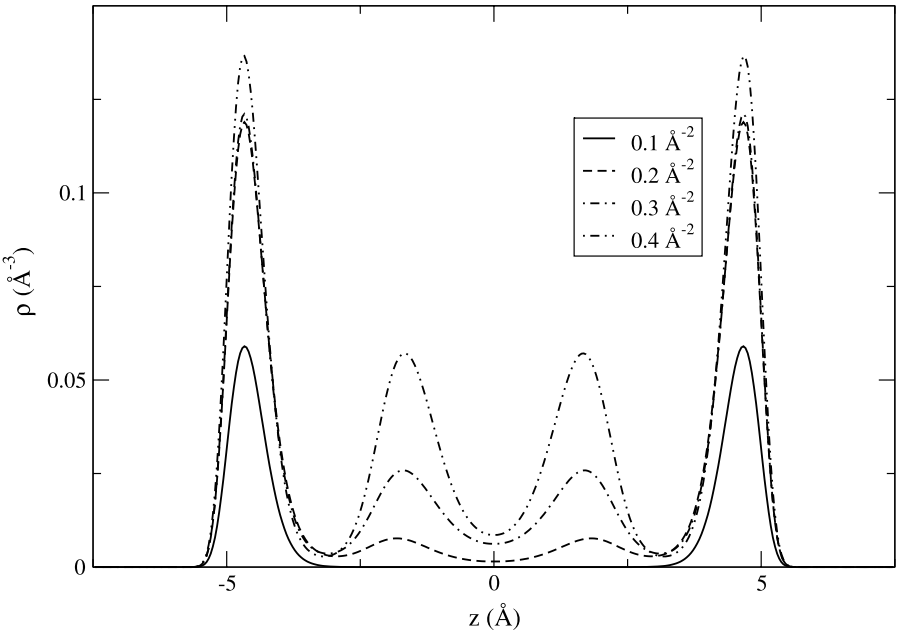

Fig. 12 Same as Fig. 10 for a width of 15 Å

an instability associated to the building of the new pair of layers as seen in Fig. 12. The jump in coverage across this transition provokes the change of slope in the grand potential (see Fig. 8). In fact, for the current set of calculations, this is the only wall separation for which such a layering (first order) phase transition is visible. However, the growth of condensed material in this slit reaches the metastable regime, $\mu > \mu_0$, before the mass distribution is capable to reverse the force on the walls. By contrast, while a width of 20 Å is sufficient to host up to six layers, the changes in the density profiles can modify the balance between attraction and repulsion in the external field, giving rise to the aforementioned reversion of the force on the walls.

The application of these results has two alternative forms, depending on the specific pore width. In the perturbative regime, one can use the equations of the introduction to compute the small expansion or contraction associated with gas uptake. There are, however, nonperturbative solutions. For example, consider the case of a pore of width $w_0 = 8$ Å exposed to gas having $\mu = -125$ K. The data in Fig. 8 above, for example, show that the gas at this value of μ can enter a pore of width 5.5 Å for which the film contribution to Ω is about -4 K/Å^2. Thus, in this scenario, the pore could contract by 2.5 Å if the energy cost of the contraction is less than or equal to 4 K/Å^2. Any realization of this possibility is a function of the material parameters.

5 Elastic Energy of Pore

In order to determine the elastic response of the pore to the presence of the adsorbate, one needs to know the parameters characterizing the empty pore in (2). These are

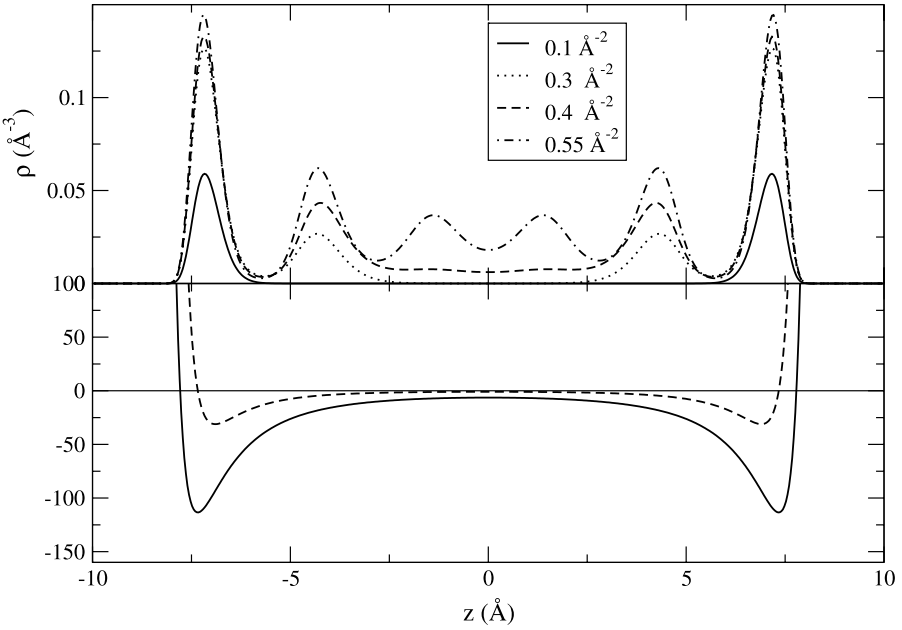

Fig. 13 Same as Fig. 10 for width 20 Å

the area A and the elastic energy quantities λ, F_0 and w_0. Manifestly, these depend on material preparation and therefore they are not known, in general. However, it is possible to characterize the behavior to lowest order and at least estimate the effects of the gas. The van der Waals (VDW) interaction energy per unit area between two identical half-spaces is given in terms of the so-called Hamaker constant $A_{\rm vdw}$ as [42]

$$V_{\rm vdw} \sim -A_{\rm vdw}/(12\pi w^2) \tag{25}$$

In the (two-body) approximation, when this energy arises from pair interactions $(-C_6/r^6)$ across the pore, expressed in terms of another VDW interaction strength C_6 and the number density n, the Hamaker constant becomes

$$A_{\rm vdw} = (n\pi)^2 C_6 \tag{26}$$

This equation, although frequently used, is a poor approximation for materials like Au and graphite, for which many-body effects (screening) are significant; a more accurate expression is used below. Now, in the case of a slit pore we must also include some repulsive "pillar energy function" $V_{\rm pillar}(w)$ which keeps the empty pore at its equilibrium separation w_0. We therefore write the total energy per unit area as

$$V(w) = V_{\rm pillar}(w) - A_{\rm vdw}/(12\pi w^2) \tag{27}$$

For simplicity, we suppose that the pillar interaction is of power-law form, expressed in terms of an unspecified length a:

$$V_{\rm pillar}(w) = [A_{\rm vdw}/(12\pi)]a^6/w^8 \tag{28}$$

(The results found below do not change significantly if the arbitrary power 8 is varied through the range 6 to 10.) Then $V(w)$ has a minimum at position w_0 with depth F_0 and second derivative (force constant) λ given by $w_0 = 4^{1/6}a$, $F_0 = A_{\rm vdw}/(16\pi w_0^2)$ and $\lambda = A_{\rm vdw}/(\pi w_0^4)$. Manifestly, these quantities are therefore determined by w_0 the input separation of the empty pore and the substrate-dependent Hamaker constant. To evaluate $A_{\rm vdw}$ numerically, we employ the general relation for low T, derived by Dzyaloshinskii et al. [43], involving $\epsilon(iE)$, the dielectric function of the material at imaginary energy iE and an integration over all real energies:

$$A_{\rm vdw} = [3/(4\pi)] \int dE \left\{ [\epsilon(iE) - 1] / [\epsilon(iE) + 1] \right\}^2 \tag{29}$$

For many materials, a simple but accurate approximation to $\epsilon(iE)$ is [38] obtained from an expression involving parameters g_0 and E_s, a characteristic energy of the solid:

$$[\epsilon(iE) - 1] / [\epsilon(iE) + 1] = g_0/[1 + (E/E_s)^2] \tag{30}$$

Inserting this into (29) yields an analytic integral result:

$$A_{\rm vdw} = 3\, E_s\, g_0^2 /16 \tag{31}$$

Inserting parameters from Appendix E of Bruch et al. [38] ($g_0 = 0.619$ and $E_s = 18.1$ eV for graphite and $g_0 = 0.84$ and $E_s = 24.2$ eV for Au) yields $A_{\rm vdw} = 1.3$ eV for graphite and $A_{\rm vdw} = 3.2$ eV for Au, the two materials used above in the numerical studies of adsorption. Together with the relation between λ, $A_{\rm vdw}$ and w_0 quoted above, one has the means to evaluate the substrate response for any assumed pore width. For example, if we consider a pore of width $w_0 = 10$ Å, then for graphite (Au), $\lambda = 0.48(1.2)$ K/Å^4.

Acknowledgements We are grateful to Angela Lueking and Silvina Gatica for helpful discussions.

This research was supported by the Department of Energy. E.S.H. acknowledges financial support through PIP 0546 from Consejo Nacional de Investigaciones Cientificas y Técnicas and X099 from University of Buenos Aires, Argentina.

References

1. C. Serre, F. Millange, C. Thouvenot, M. Nogues, G. Marsolier, D. Louer, G. Ferey, J. Am. Chem. Soc. **124**, 13519 (2002)
2. G. Ferey, M. Latroche, C. Serre, F. Millange, T. Loiseau, A. Percheron-Guegan, Chem. Commun. **24**, 2976 (2003)
3. A. Kondo, H. Noguchi, S. Ohnishi, H. Kajiro, A. Tohdoh, Y. Hattori, W.C. Xu, H. Tanaka, H. Kanoh, K. Kaneko, Nano Lett. **6**, 2581 (2006)
4. J.T. Culp, M.R. Smith, E. Bittner, B. Bockrath, J. Am. Chem. Soc. **130**, 112427 (2008)
5. A.J. Fletcher, K.M. Thomas, M.J. Rosseinsky, J. Solid State Chem. **178**, 2491 (2005)
6. D. Li, K. Kaneko, Chem. Phys. Lett. **335**, 50 (2001)
7. R. Kitaura, K. Seki, G. Akiyama, S. Kitagawa, Angew. Chem., Int. Ed. Engl. **42**, 428 (2003)
8. J.T. Culp, M.R. Smith, E. Bittner, B. Bockrath, J. Am. Chem. Soc. **130**, 12427 (2008)
9. X.B. Zhao, B. Xiao, A.J. Fletcher, K.M. Thomas, D. Bradshaw, M.J. Rosseinsky, Science **306**, 1012 (2004)

10. L.D. Gelb, K.E. Gubbins, R. Radhakrishnan, M. Sliwinska-Bartkowiak, Rep. Prog. Phys. **62**, 1573 (1999)
11. K.E. Noa, A.D. Lueking, M.W. Cole, J. Low Temp. Phys. (2010). doi:10.1007/s10909-010-0337-6
12. D.H. Bangham, N. Fakhoury, Proc. R. Soc. Lond. Ser. A, Math. Phys. Sci. **130**, 81 (1930)
13. E.O. Wiig, J. Am. Chem. Soc. **71**, 561 (1949)
14. C.H. Amberg, R. McIntosh, Can. J. Chem. **30**, 1012 (1952)
15. H.W. Quinn, R. McIntosh, Can. J. Chem. **35**, 745 (1957)
16. J.G. Dash, H. Suzanne, H. Schechter, R.E. Peierls, Surf. Sci. **60**, 411 (1976)
17. G. Reichenauer, G.W. Scherer, Colloids Surf. A **187–188**, 41 (2001)
18. T. Herman, J. Day, J. Beamish, Phys. Rev. B **73**, 094127 (2006)
19. G. Dolino, D. Bellet, C. Faivre, Phys. Rev. B **54**, 17919 (1996)
20. S. Dourdain, D.T. Britton, H. Reichert, A. Gibaud, Appl. Phys. Lett. **93**, 183108 (2008)
21. M.P. Rossi, Y. Gogotsi, K.G. Kornev, **25**, 2804 (2009)
22. G. Günther, J. Prass, O. Paris, M. Schoen, Phys. Rev. Lett. **101**, 86104 (2008)
23. A. Grosman, C. Ortega, Phys. Rev. B **B78**, 085433 (2008)
24. H.-Y. Kim, S.M. Gatica, G. Stan, M.W. Cole, J. Low Temp. Phys. **156**, 1 (2009)
25. G. Günther, M. Schoen, Phys. Chem. Chem. Phys. **11**, 9082 (2009)
26. M. Schoen, O. Paris, G. Günther, D. Müter, J. Prass, P. Fratzl, Phys. Chem. Chem. Phys. **12**, 11267 (2010)
27. A. Grosman, C. Ortega, Langmuir **25**, 8083 (2009)
28. A. Grosman, C. Ortega, Appl. Surf. Sci. **256**, 5210 (2010)
29. P.B. Balbuena, D. Berry, K.E. Gubbins, J. Phys. Chem. **97**, 937 (1993)
30. E.A. Ustinov, D.D. Do, Carbon **44**, 2652 (2006)
31. F. Ancilotto, F. Toigo, Phys. Rev. B **60**, 9019 (1999)
32. G. Mistura, F. Ancilotto, L. Bruschi, F. Toigo, Phys. Rev. Lett. **82**, 795 (1999)
33. S.M. Gatica, M.M. Calbi, M.W. Cole, Phys. Rev. E **65**, 061605 (2002)
34. R.A. Trasca, M.M. Calbi, M.W. Cole, J.L. Ricardo, Phys. Rev. E **69**, 011605 (2004)
35. Q. Wang, J.K. Johnson Int, Int. J. Thermophys. **19**, 835 (1998)
36. R. Evans, U.M. Bettolo Marconi, P. Tarazona, J. Chem. Soc. Faraday Trans. I **82**, 1763 (1986)
37. K. Morishige, H. Fujii, M. Uga, D. Kinukawa, Langmuir **13**, 3494 (1997)
38. L.W. Bruch, M.W. Cole, E. Zaremba, *Physical Adsorption: Forces and Phenomena* (Dover, Mineola, 2007)
39. F. Dalfovo, A. Lastri, L. Pricaupenko, S. Stringari, J. Treiner, Phys. Rev. B **52**, 1193 (1995)
40. E.S. Hernández, M.W. Cole, M. Boninsegni, Phys. Rev. B **68**, 1254181 (2003)
41. E.S. Hernández, J. Low Temp. Phys. **137**, 89 (2004)
42. V.A. Parsegian, *Van der Waals Forces* (Cambridge University Press, Cambridge, 2008)
43. I.E. Dzyaloshinskii, E.M. Lifshitz, L.P. Pitaevskii, Adv. Phys. **10**, 165 (1961)